JOURNAL OF GEOPHYSICAL RESEARCH, VOL. 113, A11104, doi:10.1029/2008JA013294, 2008

Suprathermal electron evolution in a Parker spiral magnetic field

M. J. Owens,[1,2] N. U. Crooker,[1] and N. A. Schwadron[1]

Received 9 April 2008; revised 8 September 2008; accepted 19 September 2008; published 15 November 2008.

[1] Suprathermal electrons (>70 eV) form a small fraction of the total solar wind electron density but serve as valuable tracers of heliospheric magnetic field topology. Their usefulness as tracers of magnetic loops with both feet rooted on the Sun, however, most likely fades as the loops expand beyond some distance owing to scattering. As a first step toward quantifying that distance, we construct an observationally constrained model for the evolution of the suprathermal electron pitch-angle distributions on open field lines. We begin with a near-Sun isotropic distribution moving antisunward along a Parker spiral magnetic field while conserving magnetic moment, resulting in a field-aligned strahl within a few solar radii. Past this point, the distribution undergoes little evolution with heliocentric distance. We then add constant (with heliocentric distance, energy, and pitch angle) ad-hoc pitch-angle scattering. Close to the Sun, pitch-angle focusing still dominates, again resulting in a narrow strahl. Farther from the Sun, however, pitch-angle scattering dominates because focusing is effectively weakened by the increasing angle between the magnetic field direction and intensity gradient, a result of the spiral field. We determine the amount of scattering required to match Ulysses observations of strahl width in the fast solar wind, providing an important tool for inferring the large-scale properties and topologies of field lines in the interplanetary medium. Although the pitch-angle scattering term is independent of energy, time-of-flight effects in the spiral geometry result in an energy dependence of the strahl width that is in the observed sense although weaker in magnitude.

Citation: Owens, M. J., N. U. Crooker, and N. A. Schwadron (2008), Suprathermal electron evolution in a Parker spiral magnetic field, *J. Geophys. Res.*, *113*, A11104, doi:10.1029/2008JA013294.

1. Introduction

[2] Solar wind electron velocity distributions can typically be divided into three main components: a thermal "core," an isotropic suprathermal (i.e., >70 eV) population called the "halo," and a suprathermal population sharply aligned with the heliospheric magnetic field called the "strahl" [*Feldman et al.*, 1975; *Rosenbauer et al.*, 1977]. While suprathermal electrons only constitute a small fraction of the total solar wind electron density, they are of key interest because the strahl acts as an effective tracer of heliospheric magnetic field topology, with a single strahl indicating open magnetic flux and counterstreaming electrons (CSEs) signaling the presence of closed magnetic loops with both foot points rooted at the Sun [e.g., *Gosling et al.*, 1987]. The picture is complicated, however, by the presence of pitch-angle scattering of suprathermal electrons. As the apex of a closed loop moves antisunward, in-transit scattering on the increasingly longer field-line will result in eventual loss of the sunward beam, and hence, loss of the CSE signature [e.g., *Owens and Crooker*, 2007]. The distance into the heliosphere a loop can travel before the CSE signature is lost depends upon the pitch-angle scattering rate and has important implications for the interpretation of the solar cycle evolution of the heliospheric magnetic field [*Owens and Crooker*, 2006, 2007].

[3] In this study we take a first step toward quantifying the CSE fade-out distance by constructing an observationally constrained model of the evolution of suprathermal electron pitch-angle distributions on open field lines. Section 2 provides a brief overview of the key observational constraints on the pitch-angle scattering mechanism. Section 3 describes the model, section 4 matches the model scattering to the observed electron evolution, and the implications of our findings are discussed in section 5.

2. Background

[4] Suprathermal electrons are generated in the corona, probably by wave-particle interactions [e.g., *Vocks et al.*, 2008], before escaping the electrostatic potential of the Sun because of their high mobility [*Pierrard et al.*, 2001]. With increasing distance from the Sun, collisions soon become infrequent enough that suprathermal electron energy and magnetic moment are conserved, resulting in a narrow field-aligned strahl as the suprathermal electrons move into a weakening magnetic field. Further out in the heliosphere, however, the presence of halo electrons and the observed

[1]Center for Space Physics, Boston University, Boston, Massachusetts, USA.
[2]Now at Space and Atmospheric Physics, Blackett Laboratory, Imperial College, London, UK.

0148-0227/08/2008JA013294$09.00

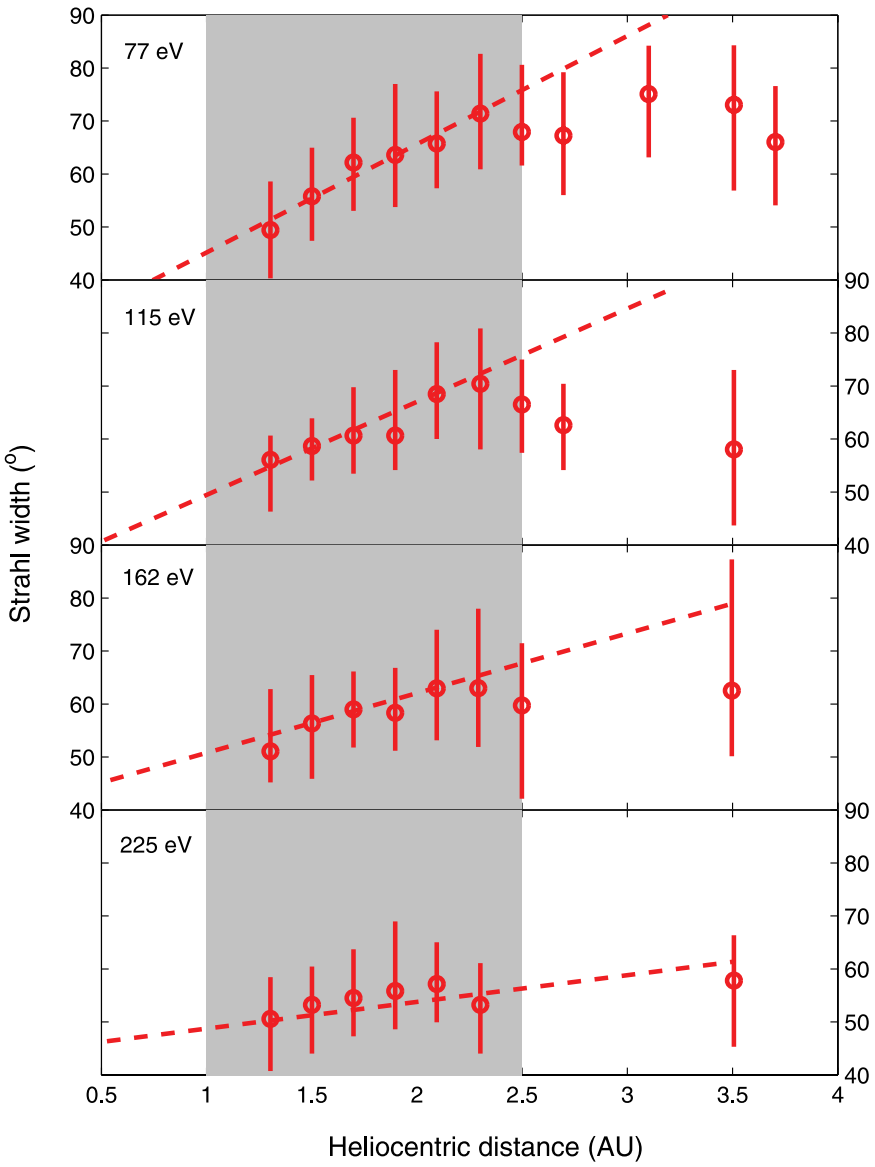

Figure 1. Ulysses observations of the suprathermal electron strahl width as a function of heliocentric distance. Red dashed lines show the best linear fits to the data. Gray-shaded regions show the range of heliocentric distances at which the strahl width is reported to increase linearly with distance. Adapted from *Hammond et al.* [1996].

width of the strahl suggest pitch-angle scattering acts during their transit. In this section we briefly summarize the observational constraints that can be placed on the suprathermal electron pitch-angle scattering mechanism. The underlying physical processes [e.g., *Gary and Saito*, 2007; *Saito and Gary*, 2007] can be better constrained by establishing unambiguously whether or not scattering has explicit distance-, heliolatitude-, and/or energy dependencies

[5] Observations indicate that the normalized core density remains constant with heliocentric distance but that strahl density decreases while halo density increases, suggesting that the halo population consists of electrons that have been pitch-angle (PA) scattered out of the strahl [*Gosling et al.*, 2001; *Maksimovic et al.*, 2005], most likely by wave-particle interactions.

[6] *Hammond et al.* [1996] used fast solar wind data from the Ulysses southern polar pass to characterize the evolution of suprathermal electrons with heliocentric distance. They fit the suprathermal electron pitch-angle distributions with the following form:

$$j(\alpha) = K_0 + K_1 \exp\left[\frac{-\alpha^2}{K_3}\right] \quad (1)$$

where $j(\alpha)$ is the differential electron flux, K_0 describes the electron density of the halo and K_3 determines the width of the strahl (the full width at half maximum is given by $FWHM = 2\sqrt{(\ln 2)K_3}$). K_1 is the maximum electron density of the strahl above the background level.

[7] Between radial distances of 1 and 2.5 AU from the Sun, *Hammond et al.* [1996] reported a positive linear correlation between suprathermal strahl width and heliocentric distance for a range of electron energies (77, 115, 162 and 225 eV), as shown in Figure 1. At heliocentric distances

greater than 2.5 AU, there may be some evidence of strahl widths decreasing with distance, though data are sparse, particularly for higher energy electrons. For 77 eV suprathermal electrons, Hammond et al. found the best linear fit to the width of the strahl as a function of heliocentric distance between 1 and 2.5 AU is given by:

$$FWHM = (27 \pm 26)^\circ + R(22 \pm 15)^\circ/AU \quad (2)$$

where R is the heliocentric distance in AU. This relation is shown as the red dashed line in Figure 1 (top). Since focusing must dominate close to the Sun to form the observed strahls, this increase in strahl width was interpreted as evidence of an increase in suprathermal electron scattering with heliocentric distance.

[8] It is important to note that the relation in equation (2) was obtained using observations gathered over a large range of heliographic latitudes, from +30° to −50°. *Hammond et al.* [1996] concluded that the amount of suprathermal electron scattering is a function of radial distance and not heliolatitude, at least inside 2.5 AU. *Scime et al.* [2001] also reported no latitudinal trends in suprathermal electron behavior once the radial variation is removed. The decrease in strahl widths at distances greater 3 AU, however, was attributed to a possible latitudinal effect, with Hammond et al. speculating that heliolatitude variations may exist, but be undetectable in their data set. In this study we investigate the evolution of the suprathermal electron strahl with heliocentric distance when the scattering term is constant with distance and latitude and compare this behavior with the observations.

[9] On the basis of observations at 1 AU, there have been conflicting findings regarding the energy-dependence of the strahl width. Both negative [*Pilipp et al.*, 1987; *Ogilvie et al.*, 2000; *de Koning et al.*, 2007] and positive [*Pagel et al.*, 2005, 2007] correlations between suprathermal electron anisotropy (which increases as the strahl narrows) and energy have been reported, meaning it is currently unclear whether there is an intrinsic energy dependence in the scattering mechanism. Using Ulysses data, ham96 plotted observed strahl widths against heliocentric distance at four electron energies. They found that best linear fits to these variations yield widths at 1 AU that increase with energy, in agreement with *Pagel et al.* [2005, 2007]. *Hammond et al.* [1996] also used the fits to show that higher energy electrons undergo less strahl broadening past 1 AU:

$$\frac{d(FWHM)}{d(R)} = 30(^\circ/AU) - 0.1E(^\circ/AU/eV) \quad (3)$$

where E is the electron energy, in eV. In this study we investigate how much of this energy-dependence can be explained by time-of-flight effects that arise even when the scattering term is independent of energy.

3. Modeling Suprathermal Electron Evolution

[10] In order to match the observed strahl broadening of suprathermal electrons with heliocentric distance, we construct a numerical model in which the time evolution of heliocentric distance (R) and pitch angle (α) of electrons are subject to two processes: Adiabatic focusing and pitch-angle scattering. We first consider adiabatic focusing in the absence of scattering.

3.1. Adiabatic Focusing

[11] The radial speed, V_R, of an electron consists of two components: advection with the radially flowing ambient solar wind and streaming along the magnetic field, independent of the ambient solar wind. Thus at a heliocentric distance R:

$$\begin{aligned} V_R(R,\alpha,\theta) &= V_{SW} + V_\parallel(R,\alpha)\cos\gamma(R,\theta) \\ &= V_{SW} + \left(\sqrt{\frac{2E}{m_e}}\cos\alpha(R)\right)\cos \\ &\quad \cdot \left(\arctan\left[\frac{2\pi}{T_{ROT}V_{SW}}R\cos\theta\right]\right) \end{aligned} \quad (4)$$

where V_{SW} is the ambient solar wind speed, $V_\parallel(R, \alpha)$ is the component of the electron speed along the magnetic field direction and $\gamma(R, \theta)$ is the angle the magnetic field makes with the radial direction. The second line expresses $V_\parallel$ in terms of E, the total electron energy, and α, the electron pitch angle relative to the magnetic field (with 0° being a completely field-aligned electron). The Parker spiral is expressed in terms of the ambient solar wind speed (V_{SW}), heliocentric distance (R), the solar rotation period (T_{ROT}) and the heliographic latitude (θ).

[12] In the absence of scattering, the evolution of electron pitch angle with R is governed by conservation of magnetic moment:

$$\sin^2\alpha(R) = \frac{B_{TOT}(R)\sin^2\alpha(R_0)}{B_{TOT}(R_0)} \quad (5)$$

where $B_{TOT}(R)$ is the magnetic field strength at distance R and R_0 represents a reference heliocentric distance. Thus to calculate the pitch-angle evolution, a model of magnetic field strength variation with heliocentric distance is required. Magnetic flux conservation through heliocentric spheres means the radial component of heliospheric magnetic field strength must fall off as $1/R^2$. In the Parker spiral model of the solar wind, the azimuthal component of the field is given by $B_\gamma(R, \theta) = B_r(R)\tan\gamma(R,\theta)$. There is no meridional field component.

[13] To find the heliocentric distance and pitch angle of an electron at a time t, we numerically integrate equations (4) and (5).

3.1.1. Model Grid

[14] Our simulation of suprathermal electrons in the solar wind uses a uniform numerical grid in electron pitch-angle cosine ($\mu = \cos\alpha$) and heliocentric distance phase space. The advantage of using a uniform μ grid, rather than a uniform pitch-angle grid, is that a flat distribution of electrons in μ-space is isotropic. The separation of grid cells in radial distance, dR, is given by R_{MAX}/NR_{MAX}, where R_{MAX} is the heliocentric distance of the outer grid boundary and NR_{MAX} is the number of grid cells in the R direction. For computation efficiency, we want to set dR as high as possible, however, dR must be set low enough to resolve the PA change which results from equation (5) in a single time-step, dt. In this study we set R_{MAX} to 8 AU and NR_{MAX} to 1600, since higher spatial resolutions are found

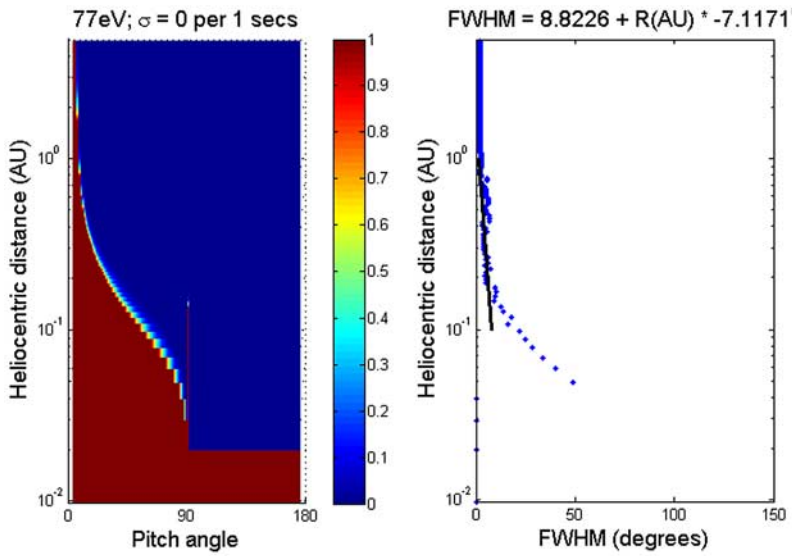

Figure 2. A numerical simulation of suprathermal electron strahl evolution with no pitch-angle scattering. (left) Suprathermal electron number density in pitch-angle and heliocentric distance phase space as a normalized color scale. (right) Full-width half-maximum (FWHM) of the strahl as a function of distance. Note the logarithmic scale on the y axis, chosen to highlight near-Sun evolution. A narrow strahl is formed within 0.5 AU, beyond which the electron distribution undergoes little evolution.

to give nearly identical results. The maximum radial speed of an electron will occur for $\alpha = 0°$ and where $\gamma = 0°$. From equation (4), This is adequate to resolve pitch-angle changes on the scale of the adopted time step.

[15] To initialize the simulation, the number of electrons in each grid cell is set to zero, except for cells at 1 R_S, which are set to have N_{INIT} electrons at all μ and all times, representing an isotropic source of suprathermal electrons near the Sun. At each time-step, we calculate the new position and for each grid cell, in accordance with equations (4) and (5). When the new heliocentric distance or μ falls at some intermediate value between two grid cells (as will usually be the case), the electrons are split between the bounding grid cells by linear interpolation. This leads to a fairly diffusive scheme, but it is adequate for our requirements, as demonstrated in the next section. Electrons propagating to the end of the simulation grid are lost. Consequently, although simulations are run out to 8 AU, back-scattered electrons are not well simulated beyond 5 AU, and results beyond this distance are not used.

3.1.2. Results With No Scattering

[16] Figure 2 shows the result of propagating suprathermal electrons through our model in the absence of pitch-angle scattering. Only adiabatic effects are present. The simulation was performed in the ecliptic plane (i.e., $\theta = 0°$). The snapshot is shown after 8000 time-steps, when electrons have propagated the full length of the simulation domain and the model has reached a steady-state equilibrium. The color scale on the left shows suprathermal electron number density, normalized to the maximum density at each radial distance, as a function of pitch angle and heliocentric distance. While the absolute value of this normalized density is determined by the arbitrarily chosen value of N_{INIT}, the density of the initial isotropic distribution, variations in this normalized density are directly comparable to variations in this normalized density are directly comparable to variations in electron differential flux, $j(\alpha)$, as observed by spacecraft. The right shows the full-width half-maximum (FWHM) of the strahl as a function of distance (this is obtained from a fit to the electron pitch-angle distribution, as described in section 2). Note the logarithmic scale in heliocentric distance, chosen to highlight near-Sun evolution. A narrow strahl is formed within 0.5 AU, beyond which the electron distribution does not undergo any further significant evolution.

[17] Figure 2 also shows a build-up of 90° pitch-angle electrons close to the Sun, as indicated by the narrow spike at that pitch angle. This population is a remnant of the 90° pitch-angle electrons in the near-Sun isotropic source, which propagate outward at the solar wind speed and thus undergo adiabatic focusing very slowly. Furthermore, even in the absence of explicit scattering, numerical diffusion means that a small fraction of the $\alpha = 90°$ electrons at can reach $\alpha > 90°$ phase space. These electrons will then propagate back toward the Sun, adiabatically defocussing as they move into stronger magnetic fields and thus repopulating the $\alpha = 90°$ phase space close to the Sun.

3.2. Adding Pitch-Angle Scattering

[18] In this section, suprathermal electron pitch-angle scattering is added to the numerical scheme outlined in the previous section. As the physical processes responsible for suprathermal electron scattering remain a topic of research, we simulate pitch-angle scattering in an ad-hoc fashion by broadening the electrons in each grid cell and at each time step by a Gaussian function of μ. Once the electrons have been pitch-angle scattered, they are subject to the same adiabatic focusing as in the previous section.

[19] To implement this scheme, we assume that if at time step i there are N_0 electrons in the μ grid cell centered at μ_0,

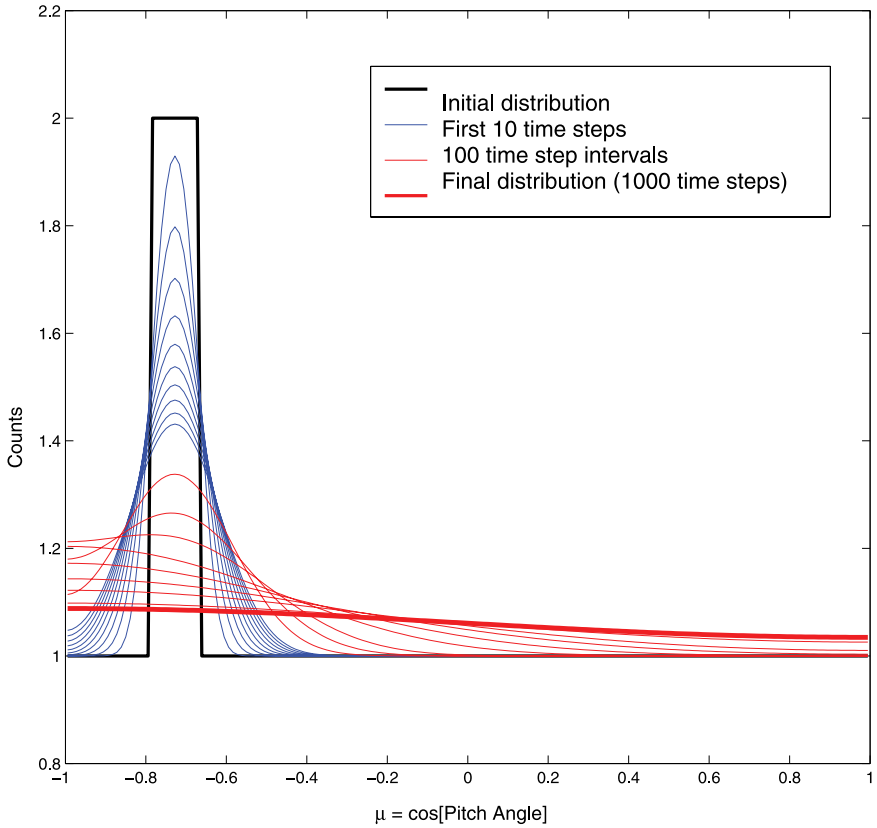

Figure 3. An example of the ad hoc pitch-angle scattering employed in this study. An initial distribution with a sharp peak centered at $\mu = -0.7$ ° (the thick black line) is time evolved with only pitch-angle scattering acting (i.e., at a fixed radial distance with no adiabatic effects). At each time step, each μ bin is broadened by a Gaussian factor of $\sigma = 0.0022$. The thin blue lines show the first 10 time steps. The thin red lines show the distribution at intervals of 100 time steps. The thick red line shows the μ distribution after 1000 time steps, as it approaches isotropy.

at time step $i + 1$ these electrons will be spread in μ by the following equation,

$$\frac{dN(\mu)}{d\mu} = \frac{N_0}{\sigma\sqrt{2\pi}} \exp\left[-\frac{(\mu-\mu_0)^2}{2\sigma^2}\right],$$

where the number of electrons is conserved,

$$N_0 = \int_{-1}^{1} d\mu \, \frac{dN}{d\mu}.$$

Thus as σ increases, the level of scattering increases, and electrons are spread over a larger range of pitch-angle cosines.

[20] In order to avoid edge effects and ensure the pitch-angle distribution tends toward isotropy, it is necessary to mirror the distribution about $\mu = \pm 1$. A similar mirroring of the distribution was performed in the data analysis of *Hammond et al.* [1996]. The total scattered pitch-angle distribution is then obtained by summing over the Gaussian distributions derived from the individual μ bins. An example of the pitch-angle scattering is shown in Figure 3, where an initial distribution (the thick black line) with a sharp peak centered at $\mu = -0.7$ ° is time-evolved with only pitch-angle scattering acting (i.e., at a fixed radial distance with no adiabatic effects). At each time step, each μ bin is broadened by a Gaussian factor of $\sigma = 0.0022$. The thin blue lines show the first 10 time steps. The thin red lines show the distribution at intervals of 100 time steps. The thick red line shows the μ distribution after 1000 time steps: it is clearly approaching an isotropic distribution.

[21] In this study, σ is a constant for each simulation; that is, the scattering rate is independent of time, heliocentric distance and electron energy. Figure 4 shows the same simulation as Figure 2 but with the addition of scattering at the Figure 3 level of $\sigma = 0.0022$. It is the same format as Figure 2 but uses a linear scale for the y axis. The near-Sun evolution is nearly identical to the no scattering case: A narrow strahl forms within 0.1 AU, indicating adiabatic focusing overwhelms pitch-angle broadening resulting from scattering. However, past 0.5 AU the strahl begins to broaden significantly, indicating a dominance of pitch-angle scattering over adiabatic focusing. This is clear in both the color-coded pitch-angle distributions on the left and the blue FWHM curve on the right. The red points on the right show the width of the strahl obtained from Ulysses observations [*Hammond et al.*, 1996]. These provide an excellent fit to the blue curve in the gray-shaded range of 1–2.5 AU, as discussed further in section 4. Note that the same scattering

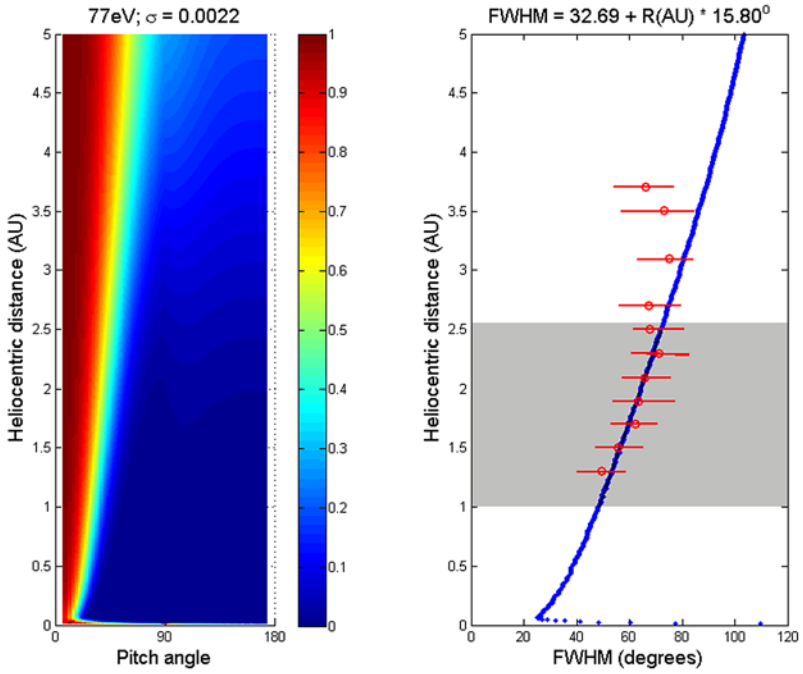

Figure 4. A numerical simulation of suprathermal electron strahl evolution with ad-hoc pitch-angle scattering (σ = 0.0022), in the same format as Figure 2, but with a linear y axis. As in the case of no scattering, a narrow strahl is formed by 0.1 AU. However, the strahl then broadens significantly between 1 and 5 AU despite the fact that the scattering function has no explicit dependence on heliocentric distance. The red points in the right show the width of the strahl obtained from Ulysses observations [*Hammond et al.*, 1996].

rate was used at all heliocentric distances. Thus this simulation clearly demonstrates that adiabatic focusing can dominate close to the Sun while scattering can take over at larger heliocentric distances, even when there is no explicit R-dependence in the scattering rate.

4. Matching Observations

[22] In this section, we vary the ad-hoc scattering rate to best match the observed suprathermal electron evolution reported by [*Hammond et al.*, 1996]. We begin by matching the observations of strahl broadening for 77 eV electrons. Ideally, the scattering parameter, σ, would be varied in the simulations to fit the observations as a function of three parameters: heliocentric distance, pitch angle, and heliolatitude. However, the uncertainties in the current observational analysis are too large for such a method to provide a meaningful result. Instead, since *Hammond et al.* [1996] and *Scime et al.* [2001] found no heliolatitude dependence to the suprathermal electron behavior, we investigate the broadening of the strahl width at a fixed heliographic latitude of 0° (i.e., approximately in the ecliptic plane). We use a solar wind speed of 800 km/s, as the Hammond et al. observations were limited to the fast solar wind. The resulting model pitch-angle distributions are fit in the same manner as in the *Hammond et al.* [1996] analysis of the Ulysses observations (see section 2).

[23] For 77 eV electrons we find that a Gaussian scattering broadening of 0.0022 applied every time step gives a close match to observations, as shown in Figure 4 (right). This scattering rate is then applied to 115, 162 and 225 eV electrons. The resulting strahl widths as a function of heliocentric distance are shown in Figure 5 as solid black lines. Higher (σ = 0.0027, the black dashed lines) and lower (σ = 0.0017, the black dotted lines) scattering rates are shown for reference. The red points show the width of the strahl obtained from Ulysses observations, while the grey shaded region shows the heliocentric distances at which *Hammond et al.* [1996] reported a linear increase in strahl width. A constant scattering rate of σ = 0.0022 is able to match the majority of the observations within the error bars.

[24] Even with a scattering rate independent of energy, an energy dependence to the strahl width still arises in the simulations, in same sense as that observed, solely from time-of-flight effects: The scattering rate is constant, but for a given pitch angle, higher energy electrons will move a greater radial distance per unit of time, resulting in greater adiabatic focusing. For the 0.0022 scattering factor, we find the following energy dependence:

$$\frac{d(FWHM)}{d(R)} = 17(^\circ/AU) - 0.013E(^\circ/AU/eV) \qquad (6)$$

[25] The magnitude of the modeled energy dependence is much weaker than the best fit by *Hammond et al.* [1996], despite matching most of the observational data points within the large uncertainty. The match for higher-energy electrons in Figure 5, however, is systematically off, moving from the bottom of the error bars upward with increasing heliocentric distances, consistent with the weaker modeled energy dependence. Further observations are clearly required

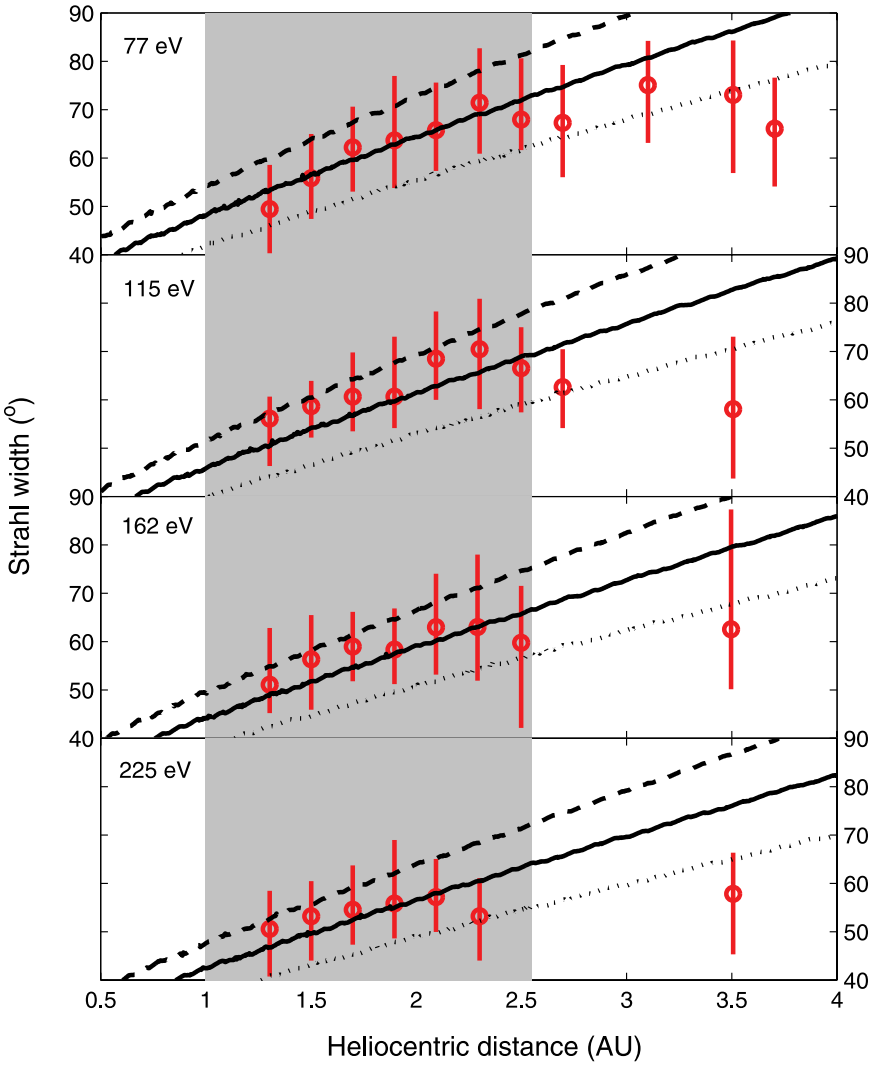

Figure 5. Suprathermal electron strahl width as a function of heliocentric distance for various electron energies, in the same format as Figure 1. Solid black lines show the results of numerical simulations of electron evolution with pitch-angle scattering tuned to match the 77 eV electron observations (i.e., σ = 0.0022). Model results for higher (σ = 0.0027, the black dashed lines) and lower (σ = 0.0017, the black dotted lines) scattering rates are also shown for comparison. A constant scattering rate of σ = 0.0022 matches the majority of the observations within the observational uncertainties, although the decrease in the gradient of the strahl width-distance relation with energy does not seem as marked as observed.

to conclusively determine if there is an explicit energy dependence in the scattering mechanism.

5. Discussion

[26] Suprathermal solar wind electrons are observed to form a narrow strahl close to the Sun, but the strahl broadens with heliocentric distance, presumably owing to pitch-angle scattering opposing the tendency to focus through conservation of magnetic moment. Via simple numerical simulations of suprathermal electrons in a Parker spiral magnetic field with an ad-hoc parameterization of pitch-angle scattering, we find this behavior naturally arises without an explicit distance dependence in the scattering mechanism.

[27] The reason for the switch from focusing to scattering in the model is a simple geometric effect of the Parker spiral magnetic field, as shown in Figure 6. For a given energy and pitch angle, an electron has a particular speed along the magnetic field. Close to the Sun, the field is almost radial, giving the electron a nearly radial velocity. With distance from the Sun the angle between the heliospheric magnetic field and the radial direction increases, reducing the radial component of an electron's velocity: In a given time period, an electron travels a smaller radial distance the further it is from the Sun. Thus the focusing rate drops off with radial distance, allowing scattering to become the dominant process at large R, even though the scattering itself is independent of R. We note that this effect should decrease with increasing heliolatitude, as the spiral field becomes less tightly wound. Such an effect has not been reported in the observations, though it is difficult to separate distance and latitude variations in the Ulysses data. This effect may merit further investigation.

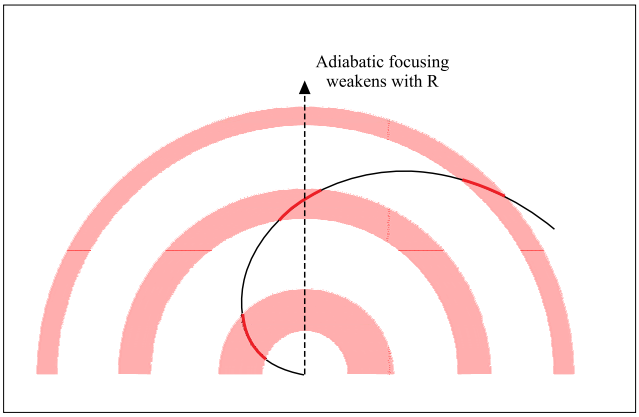

Figure 6. An explanation for the switch from suprathermal focusing to strahl broadening with a constant scattering rate. The thick red intervals along the spiral field line show the distance an electron of a given energy can move in a fixed unit of time, with red-shaded regions showing the associated change in heliocentric distance. Close to the Sun, field lines are nearly radial so that electrons experience a large change in R and field strength per unit time and, thus, strong adiabatic focusing. Far from the Sun, the angle between the field and the radial direction is much larger so that electrons experience a smaller change in field strength per unit time and weaker focusing. Consequently, the strahl broadens at greater heliocentric distances, although the scattering rate is constant.

[28] The simulations also show how time-of-flight effects can result in the observed sense of energy dependence in the strahl width even when the scattering rate is constant. Quantitatively, however, we find this effect to be weaker than observed, suggesting the existence of an explicit energy dependence in the pitch-angle scattering mechanism, with higher energy electrons undergoing less scattering, in line with the 1-AU findings of *Pagel et al.* [2005, 2007], but contrary to *Pilipp et al.* [1987], *Ogilvie et al.* [2000], and *de Koning et al.* [2007]. The large uncertainty in the *Hammond et al.* [1996] observations, however, makes a definitive statement difficult. Further analysis of the available Ulysses observations are required to conclusively determine the energy dependence of the scattering process.

[29] Finally we note the possibility of heliospheric magnetic field lines being significantly longer [*Ragot*, 2006] or shorter [*Pei et al.*, 2006] than predicted by the Parker model of the solar wind. Such effects would alter the scattering rate required to match the observed strahl width. Furthermore, for a constant scattering rate, it should change the energy and latitude variations with strahl width. With additional modeling and observations of suprathermal electrons, it may be possible to place constraints on field-line length and hence on turbulent processes in the solar wind. Thus by determining the amount of scattering required to explain the electron distributions at the Ulysses spacecraft between 3 and 5 AU from the Sun, our model provides an important tool that can be utilized in future studies of electron distributions to infer the large-scale properties and topologies of field lines in the interplanetary medium.

[30] **Acknowledgments.** This research was supported by the National Science Foundation under Agreement ATM-012950, which funds the CISM project of the STC program, and under grant ATM-0553397. M.O. thanks Harlan Spence, Mike Golightly, Chia-Lin Huang, and Slava Merkin of Boston University, and Tim Horbury and Steve Schwartz of Imperial College for useful discussions.

[31] Amitava Bhattacharjee thanks John Steinberg and another reviewer for their assistance in evaluating this paper.

References

de Koning, C. A., J. T. Gosling, R. M. Skoug, and J. T. Steinberg (2007), Energy dependence of electron pitch angle distribution widths in solar bursts, *J. Geophys. Res.*, *112*, A04101, doi:10.1029/2006JA011971.

Feldman, W. C., J. R. Asbridge, S. J. Bame, M. D. Montgomery, and S. P. Gary (1975), Solar wind electrons, *J. Geophys. Res.*, *80*, 4181–4196.

Gary, S. P., and S. Saito (2007), Broadening of solar wind strahl pitch-angles by the electron/electron instability: Particle-in-cell simulations, *Geophys. Res. Lett.*, *34*, L14111, doi:10.1029/2007GL030039.

Gosling, J. T., D. N. Baker, S. J. Bame, W. C. Feldman, and R. D. Zwickl (1987), Bidirectional solar wind electron heat flux events, *J. Geophys. Res.*, *92*, 8519–8535.

Gosling, J. T., R. M. Skoug, and W. C. Feldman (2001), Solar wind electron halo depletions at 90° pitch angle, *Geophys. Res. Lett.*, *28*, 4155–4158.

Hammond, C. M., W. C. Feldman, D. J. McComas, J. L. Phillips, and R. J. Forsyth (1996), Variation of electron-strahl width in the high-speed solar wind: ULYSSES observations, *Astron. Astrophys.*, *316*, 350–354.

Maksimovic, M., et al. (2005), Radial evolution of the electron distribution functions in the fast solar wind between 0.3 and 1.5 AU, *J. Geophys. Res.*, *110*, A09104, doi:10.1029/2005JA011119.

Ogilvie, K. W., R. Fitzenreiter, and M. Desch (2000), Electrons in the low-density solar wind, *J. Geophys. Res.*, *105*, 27,277–27,288.

Owens, M. J., and N. U. Crooker (2006), Coronal mass ejections and magnetic flux buildup in the heliosphere, *J. Geophys. Res.*, *111*, A10104, doi:10.1029/2006JA011641.

Owens, M. J., and N. U. Crooker (2007), Reconciling the electron counter-streaming and dropout occurrence rates with the heliospheric flux budget, *J. Geophys. Res.*, *112*, A06106, doi:10.1029/2006JA012159.

Pagel, C., N. U. Crooker, D. E. Larson, S. W. Kahler, and M. J. Owens (2005), Understanding electron heat flux signatures in the solar wind, *J. Geophys. Res.*, *110*, A01103, doi:10.1029/2004JA010767.

Pagel, C., S. P. Gary, C. A. de Koning, R. M. Skoug, and J. T. Steinberg (2007), Scattering of suprathermal electrons in the solar wind: ACE observations, *J. Geophys. Res.*, *112*, A04103, doi:10.1029/2006JA011967.

Pei, C., J. R. Jokipii, and J. Giacalone (2006), Effect of a random magnetic field on the onset times of solar particle events, *Astrophys. J.*, *641*, 1222–1226, doi:10.1086/427161.

Pierrard, V., M. Maksimovic, and J. Lemaire (2001), Self-consistent model of solar wind electrons, *J. Geophys. Res.*, *106*, 29,305–29,312.

Pilipp, W. G., K.-H. Muehlhaeuser, H. Miggenrieder, H. Rosenbauer, and R. Schwenn (1987), Variations of electron distribution functions in the solar wind, *J. Geophys. Res.*, *92*, 1103–1118.

Ragot, B. R. (2006), Lengths of wandering magnetic field lines in the turbulent solar wind, *Astrophys. J.*, *653*, 1493–1498, doi:10.1086/508872.

Rosenbauer, H., et al. (1977), A survey on initial results of the HELIOS plasma experiment, *J. Geophys.*, *42*, 561–580.

Saito, S., and S. P. Gary (2007), All whistlers are not created equally: Scattering of strahl electrons in the solar wind via particle-in-cell simulations, *Geophys. Res. Lett.*, *34*, L01102, doi:10.1029/2006GL028173.

Scime, E. E., J. E. Littleton, S. P. Gary, R. Skoug, and N. Lin (2001), Solar cycle variations in the electron heat flux: Ulysses observations, *Geophys. Res. Lett.*, *28*, 2169–2172.

Vocks, C., G. Mann, and G. Rausche (2008), Formation of suprathermal electron distributions in the quiet solar corona, *Astron. Astrophys.*, *480*, 527–536, doi:10.1051/0004-6361:20078826.

N. U. Crooker and N. A. Schwadron, Center for Space Physics, Boston University, 725 Commonwealth Ave., Boston, MA 02215, USA.

M. J. Owens, Space and Atmospheric Physics, Blackett Laboratory, Imperial College London, Princeton Consort Road, London SW7 2BZ, UK. (mjowens@bu.edu)